

Multi-layer film flow down an inclined plane: experimental investigation

D. Henry · J. Uddin · J. Thompson · M. G. Blyth ·
S. T. Thoroddsen · J. O. Marston

Received: 10 April 2014 / Revised: 1 October 2014 / Accepted: 6 November 2014 / Published online: 19 November 2014
© Springer-Verlag Berlin Heidelberg 2014

Abstract We report the results from an experimental study of the flow of a film down an inclined plane where the film itself is comprised of up to three layers of different liquids. By measuring the total film thickness for a broad range of parameters including flow rates and liquid physical properties, we provide a thorough and systematic test of the single-layer approximation for multi-layer films for Reynolds numbers $Re = \rho Q/\mu \approx 0.03 - 60$. In addition, we also measure the change in film thickness of individual layers as a function of flow rates for a variety of experimental configurations. With the aid of high-speed particle tracking, we derive the velocity fields and free-surface velocities to compare to the single-layer approximation. Furthermore, we provide experimental evidence of small capillary ridge formations close to the point where two layers merge and compare our experimental parameter range for the occurrence of this phenomenon to those previously reported.

1 Introduction

The applications of coating processes are vast, from traditional practices in the photographic and film industry to more modern examples such as hydrophilic coatings of medical materials (LaPorte 1997). It is well known that coating flows can be split into two classes: pre- and self-metered methods (Weinstein and Ruschak 2004), with curtain coating a particular example of a pre-metered coating, where a precise volumetric flow rate is ultimately delivered onto the substrate to be coated. In curtain coating, a freely falling liquid film accelerates under gravity before impinging onto a substrate passed underneath at high speed (up to 1,000 m/min). This technique exploits the inertia in the curtain to pin the fluid onto the substrate thus eliminating air entrainment (see Marston et al. 2007), which typically causes defects downstream in liquid film coatings. Moreover, curtain coating has been of recent interest due its major industrial advantage of being able to efficiently coat multiple layers of different fluids at the same time (Miyamoto and Katagiri 1997) and encompasses many fascinating fluid mechanical components in its process. A greater understanding of these individual sections of the flow process is critical to the development of the overall curtain coating method. In this study, we focus on the film flow of single and multiple layers, *before* the liquid forms the curtain. This occurs on the top face of the coating “die”. In our case, we employ a slide-die curtain coating facility, whereby high-precision flowmeters control the flow rate to several (in our case, up to four) inlets that evenly distribute the fluid across an exit slot onto the surface of an inclined planar surface—i.e. the “slide”. Each separate layer of fluid is then stacked on top of one another as it flows down the inclined plane due to gravity, before leaving the die at a vertical lip. Figure 1 shows a schematic representation of the flow examined herein.

D. Henry · J. Uddin
School of Mathematics, University of Birmingham,
Edgbaston B15 2TT, United Kingdom

J. Thompson · M. G. Blyth
School of Mathematics, University of East Anglia,
Norwich NR4 7TJ, United Kingdom

S. T. Thoroddsen
Division of Physical Sciences and Engineering, King Abdullah
University of Science and Technology, Thuwal 23955-6900,
Saudi Arabia

J. O. Marston (✉)
Department of Chemical Engineering, Texas Tech University,
Lubbock, TX 79409, USA
e-mail: jeremy.marston@ttu.edu

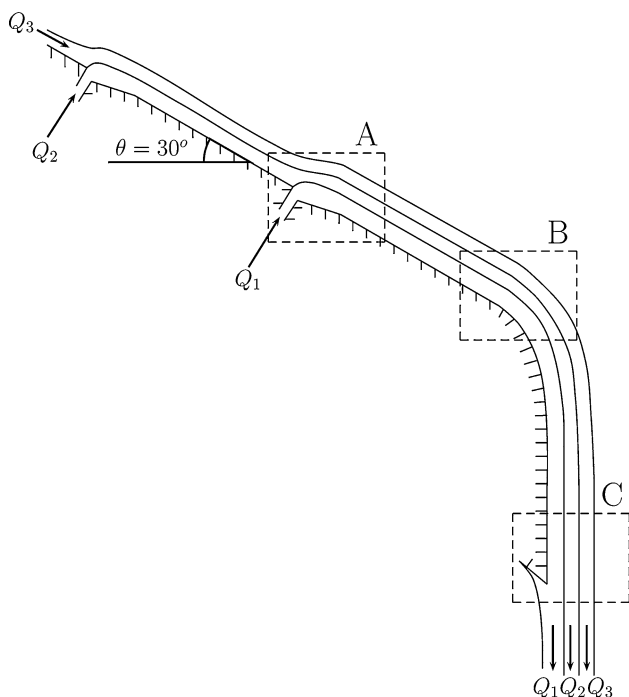


Fig. 1 Cross-sectional schematic of the formation of a three-layer film flow on a slide die. The dashed boxes mark the different viewing regions where experimental images were taken as follows: (a) the exit slot region of layer one, (b) the curvature of the die and (c) the lip where the film forms a curtain

The film flow of a single fluid, of constant properties, down a plane inclined by an angle θ , considered in the two-dimensional case (e.g. Fig. 1), has already been subject to considerable study. Nusselt (1916) first derived the exact solution to the 2-D governing equations and boundary conditions with the steady solution having a unidirectional velocity $u(y)$ and constant film thickness h , given by

$$u(y) = \frac{\rho g \sin \theta}{2\mu} y(2h - y), \quad h = \left(\frac{3\mu Q}{\rho g \sin \theta} \right)^{1/3}, \quad (1)$$

where ρ is the density, g is the acceleration due to gravity, μ is the dynamic viscosity, and Q is the flow rate per unit width. These equations can be extended to the case of multiple layers of identical fluid stacked on top of each other, which has been analysed by numerous studies, including those of Weinstein (1990) and Jiang et al. (2005), whereby the approximate film thickness and free-surface velocity are given by

$$h_T = \left(\frac{3Q_T \mu_1}{\rho_1 g \sin \theta} \right)^{1/3}, \quad U_s = \frac{\rho_1 g h_T^2 \sin \theta}{2\mu_1} \quad (2)$$

where the total volumetric flow rate per unit width $Q_T = \sum_{j=1}^n Q_j$ is simply the sum of the individual layers.

For multiple layers of identical fluid 2 holds exactly, but is an approximation for layers comprising of different fluids, where μ_1 and ρ_1 strictly refer to the viscosity and density of the layer closest to the wall. Thus, Eq. (2) gives us the “one-layer approximation” referred to throughout this work.

Of course, this approximation for the constant film thickness, in reality, is susceptible to free-surface waves as well as interfacial waves between fluid–fluid boundaries. In the light of this, there have been many studies focused on the stability of such flows following from the original works of Kapitza (1948) and Yih (1955), including those of Benjamin (1957) and Binnie (1957). In particular, Yih (1963) concluded that there is a critical Reynolds number, $Re_C = \frac{5}{6} \cot \theta$, above which free-surface waves will be amplified. These works were extended to two-layer stratified systems by Kao (1965a, b, 1968) and then further advanced by the study of wave motion in an n-layered film (Akhtaruzzaman et al. 1978; Wang et al. 1978) and an equivalent analysis for a Carreau (shear-thinning) fluid by Weinstein (1990), who determined the film thicknesses and velocity profiles in each layer.

Experimentally, numerous studies have utilised particle image velocimetry (PIV) techniques to visualise small-scale liquid film flows. Alekseenko et al. (2007) applied PIV to the flow of a single-layer film down an inclined cylinder, showing that the underside film flow obeyed the Nusselt solution, whilst Adomeit and Renz (2000) employed both PIV and fluorescence to study the film thickness and wave motion down an inclined single-layer film. Dietze et al. (2009) performed careful measurements of the film flow inside a vertical cylinder using both laser doppler velocimetry (LDV) and PIV to render high-resolution measurements of the wave interactions with the velocity fields. Wierschem et al. (2002) also applied LDV to measure the velocity in falling films. Most recently, single-layer films were studied using a simple visualisation technique by Njifenju et al. (2013) with emphasis on wave speeds for low-viscosity water films. Multi-layer film flows have been investigated by the authoritative work of Schweizer (1988). Many photographs were presented, depicting the cross-sectional liquid film profile along a slide die, showing liquid interfaces as well as internal features of the flow using hydrogen bubbles and dye injection to visualise streamlines. See also Kistler and Schweizer (1997) and Christodoulou and Scriven (1984) for examples of visualisation in coating flows. However, the film thicknesses and velocities were not documented in these studies. Jiang et al. (2005) provide some experimental data for three-layer flows of gelatine solution, with the emphasis being on the stability and wave-like structures rather than the actual film thicknesses. In addition, Noakes et al. (2002) refined the original imaging technique of Schweizer (1988) to study two-layer

flows for a range of slide-die geometries, comparing the experimental free-surface profiles and streamlines to those derived from theory, showing good agreement.

Thus, the main scope of this work is to gain experimental insight into the flow of multi-layer films down an incline plane. Specifically, to measure the total film thickness and the change in film thickness from a simple one-layer flow to that of two and three layers, as well as obtaining velocity fields for multi-layered films. In doing so, we make observations of capillary ridges and dimples in the region just prior to where two layers merge. This phenomenon has previously been documented theoretically by the works of Kalliadasis et al. (2000) and Bontozoglou and Serifi (2008), but experimental results are lacking in the literature. To our knowledge, this study is the first to document such data for multi-layer systems.

2 Experimental set-up

2.1 Slide-die geometry

For these experiments, a custom-built four-layer slide die (TSE Troller AG, Switzerland) was used. The full experimental apparatus is described in Marston et al. (2014) so that here we will describe the key components. The slide die, shown in Fig. 2, was situated on a moveable table built from aluminium profile. Below the die is an angled plate (shown at the bottom of Fig. 2) to deflect liquid emanating from the die into a stainless steel catchpan. Located next to the table housing the slide die was another unit (the “pumping station”) which housed the fluid holding tanks (four 200-l tanks), gear pumps and electromagnetic flowmeters. The pumps were able to deliver flow rates from 0.25 up to 7 l/min. The exact flow rate for each individual layer was determined by the flowmeter (Proline Promag series 50H, Switzerland) and converted into a flow rate per unit width ($\text{cm}^2 \text{s}^{-1}$). The fluid was delivered to each layer through a feed line located at the bottom of the slide die and distributed through the width of the cavities before exiting on the top face of the die. The die is 12-cm wide and is fixed at an incline of 30° to the horizontal. The exit region of each slot is approximately 5.5 mm in total length from the back of the exit slot. This geometry, shown in Fig. 3, is referred to as a “Chamfered” exit slot (Noakes et al. 2002) and was chosen specifically for its ability to produce laminar flows and to prohibit the inclusion of recirculation zones as seen by Schweizer (1988). In addition, the die face was subjected to significant polishing treatment to yield a mirror-like finish with very low surface roughness ($R_a = 0.1 \mu\text{m}$, $R_{t,max} = 1.2 \mu\text{m}$) that was easily wet by all fluids used in this study.

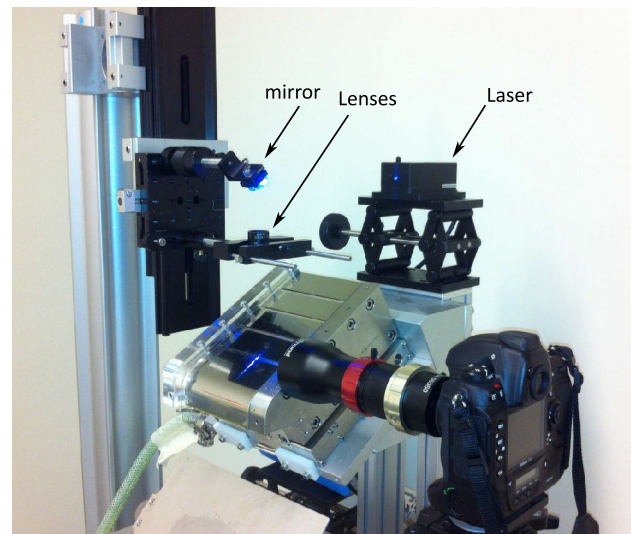


Fig. 2 Photograph of the experimental set-up, showing the die face illuminated by a blue laser passed through optics to create a light sheet

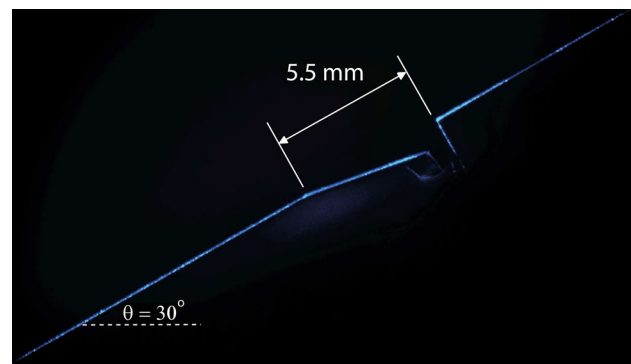


Fig. 3 Exit slot geometry for the slide die used in the experiments. The edge of the die was illuminated by the blue laser light sheet in this photograph

2.2 Flow visualisation

In order to gain quantitative information from the flow, we need to use appropriate flow visualisation techniques. Authoritative reviews on this subject are given in Schweizer (1988, 1997) and herein we use a similar method of optical sectioning, i.e. using a narrow focal depth lens focused into the plane of a light sheet deep within the film, to image a single plane near the centre of the die to minimise edge effects.

In our experiments, two different methods were used for capturing information about the flow. For obtaining the total film thickness, we used a laser-induced fluorescence technique, whereby the fluid contains fluorescein dye excited by a blue laser light (475 nm, B&W Tek Flex)

with peak absorption and emissions occurring at 494 and 520 nm, respectively. The fluorescence was captured by a high-resolution digital camera (Nikon D3X) with effective pixel resolutions down to $3.95 \mu\text{m}$, depending on the exact magnification.

In many previous studies (e.g. Portalski 1963; Salazar and Marschall 1978; Drosos et al. 2004; Njifenju et al. 2013), the measurement of instantaneous film thicknesses for low-viscosity fluids was complicated by the formation of waves, since the thickness would be fluctuating, and was circumvented by using a time-averaging filter. Here, we use long exposures, up to 1 s, without observing any blurring motion thus indicating that there are no waves present. However, as discussed in detail in Sect. 5, we do observe stationary capillary ridges.

For obtaining the velocity fields, we used the hydrogen bubble technique as used in the works of Schweizer (1988) and Noakes et al. (2002) in combination with a high-speed camera (Photron Fastcam SA-3) at frame rates up to 1,000 fps. For both types of experiment (film thickness or velocity field), the same blue laser light was used with a mirror and lens assembly (shown in Fig. 2) to render a light sheet angled down onto the face of the die.

To recapitulate, the main points of the hydrogen bubble technique are as follows: an electrical circuit incorporating the liquid film is created by using a DC power supply with a fine platinum wire ($75 \mu\text{m}$ in diameter) as the negative electrode and the die itself as the positive electrode. When the wire is lowered into the liquid film, hydrogen bubbles are created and swept along with the flow of the film, thus acting as tracer particles. Since this method relies on the conductivity of the liquid, a small amount of salt is added to the fluid and the voltage selected using guidelines from Schweizer (1988). In all cases, we carefully lowered the wire into exit slot cavity using a micrometer stage to ensure the full height of the film is seeded with the tracer bubbles. The bubbles are then illuminated with the same blue laser light sheet, and due to the highly reflective nature of the bubbles, they are easily captured by the high-speed camera with shutter speeds as low as $1/3,000$ s to minimise streaking. The diameter of the wire was chosen using the criterion $d_w < 40(\frac{3(\mu/\rho)^4}{g \cos \theta Q^2})^{1/3}$ based upon the principle that obstacles smaller than this length will not disturb the flow. Also, with reference to Schweizer (1988), the bubbles produced with this diameter wire are small enough that we can neglect the buoyancy force experienced throughout the flow of the film and thus expect them to faithfully follow the flow.

To obtain a cross-sectional profile as the fluid emanates from the exit slot and flows along the inclined plane, all still photographs and high-speed video sequences were taken from the side of the slide die with a telecentric lens arrangement (Edmund Optic Gold Series or Nikon 105 mm with multiple extension rings) which is focused into the

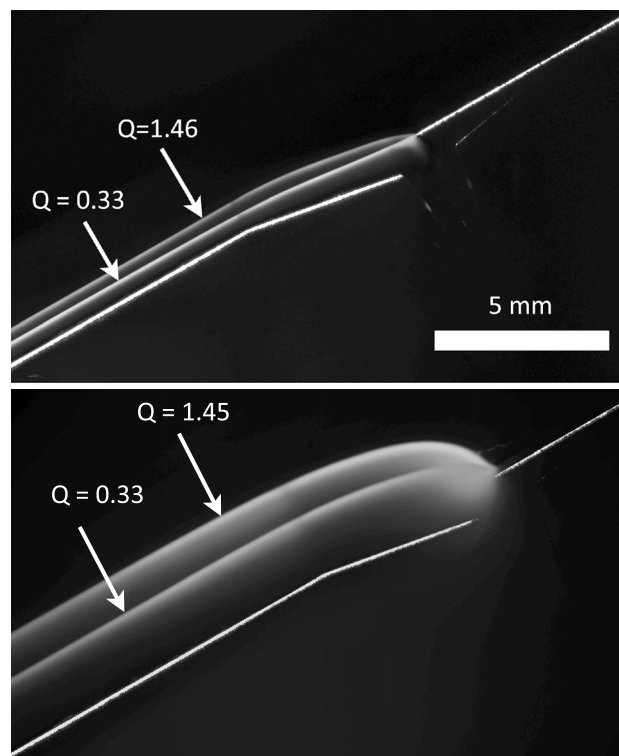


Fig. 4 Superimposed free-surface profiles for single layers of 50 % glycerol (top) and 90 % glycerol (bottom). The flow rates are given on the images along with a reference scale bar. The die face has been superimposed on the images. In (a) $Re = 4.5$ and 19.9 , in (b) $Re = 0.17$ and 0.76

plane of the laser sheet. The edge guides on the top face of the die, used primarily to constrain the fluid to the die face, were transparent and induced an upward facing meniscus, thus rendering easy optical access to the centre of the die face where the laser sheet was positioned. This technique is also detailed in Schweizer (1988).

The laser sheet is rendered by reflecting a horizontal beam at an angle off a mirror and then passing through a combination of an elliptical and cylindrical lens onto the face of the die. Before taking a set of images, a reference image with no flow is captured, such as that shown in Fig. 3. This allows us, in the analysis, to superimpose the reference image with an image of the free surface when there is film flow, meaning the film thickness and contact line position can be viewed with ease.

Figure 4 shows a comparison of the free-surface profiles obtained for two different flow rates of a single-layer film, taken at position A of Fig. 1. In these examples, $Q = 0.33$ and $1.45 \text{ cm}^2 \text{ s}^{-1}$, for two different Newtonian fluids with (a) $\mu = 8.4 \text{ mPa s}$ and (b) $\mu = 219 \text{ mPa s}$. The corresponding film thicknesses, measured at the end of the field-of-view, are (a) $h = 0.57$ and 0.91 mm and (b) $h = 1.9$ and 2.9 mm , respectively. Film thicknesses are discussed in Sect. 3.

In addition, Fig. 5 shows an example image from a high-speed video sequence for a two-layer flow, where the flow in the top is seeded with hydrogen bubbles. Again, this image is taken at point A in Fig. 1. The dashed red lines highlight the boundaries of this top layer. We will examine the velocity fields in Sect. 4.

Based on the effective spatial resolution, we estimate the error in film thickness measurements to be of the order of $\pm 20 \mu\text{m}$ (see Clarke 1995), whilst for the velocity fields, we estimate the error to be no more than 2 mm/s.

2.3 Fluid properties

The fluids used in this study were simple water–glycerol mixtures and aqueous solutions of carboxymethyl cellulose (CMC), with an average molecular weight of 90,000 g/mol and degree of substitution (DS) of 0.7. The glycerol mixtures exhibited characteristic Newtonian viscosities, whilst the CMC solutions exhibited shear-thinning properties that were best described by the cross model (e.g. Benchabane and Bekkour 2008; Chhabra and Richardson 2008), given by

$$\frac{\mu - \mu_\infty}{\mu_0 - \mu_\infty} = \frac{1}{1 + [\lambda\dot{\gamma}]^{(1-\alpha)}} \tag{3}$$

where μ is the apparent viscosity, $\dot{\gamma}$ is the shear rate, μ_0 and μ_∞ are the asymptotic values of viscosity at zero and infinite shear rates, λ is a constant with units of time and α is a rate index constant. The physical properties of the glycerol mixtures are listed in Table 1, whilst the rheological and physical properties of the CMC solutions are listed in Table 2. All viscosities and rheological measurements were made on an Ares G2 rheometer (TA instruments). In some cases, sodium dodecyl sulphate (SDS) was added to modify the surface tension.

We also note that we can neglect inter-layer diffusion since, for most cases, the layers are the same fluid. However, even when the layers are of different concentrations of water in glycerol, the diffusion coefficient is $D = O(10^{-5}) \text{cm}^2 \text{s}^{-1}$ and the timescale for diffusion is $t \sim L^2/4D = 1\text{--}4 \text{min}$ for $L \approx 1 \text{mm}$.

3 Total film thickness measurements

In Fig. 6, we plot the film thickness measured for the CMC solutions at all different concentrations used. Here, the predicted thickness from the Nusselt

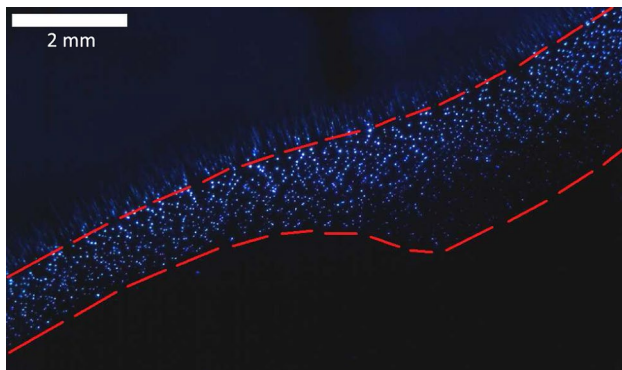


Fig. 5 Frame from a high-speed video sequence captured at 1,000 fps for a two-layer 5 % CMC solution with $Q_1 = 0.67$ and $Q_2 = 0.5 \text{cm}^2 \text{s}^{-1}$. Hydrogen bubbles are present in the top layer (Q_2) only. The dashed red line lines indicate the free surface and lower interface of the top layer ($Re = 0.13$)

Table 2 Rheological and physical properties of the CMC solutions used

CMC conc. (%w/w)	μ_0 Pa s	$\lambda (\times 10^{-3} \text{s})$	α	Surface tension (mN/m)
2	0.037	0.12	0.03	69.8
3	0.137	0.33	0.223	69.6
4	0.407	0.93	0.346	69.9
5	0.926	2.58	0.422	68.2

For all solutions, a value of $\mu_\infty = 0.001 \text{Pa s}$ was assumed for fitting to Eq. (3). The stated values were measured at the ambient temperature of the laboratory during the experiments (21 °C)

Table 1 Physical properties of the glycerol-based fluids used in the experiments

Glycerol conc. (%v/v)	Viscosity μ (mPa s)	Density ρ (kg/m ³)	Surface tension σ (mN/m)	
50	8.4	1,146	66.9	
60	15.3	1,171	65.7	
70	30	1,196	64.7	
80	72	1,218	63.7	
90	219	1,241	62.3	
~60 (0.05 SDS)	16.6	1,171	48.5	
The stated values were measured at the ambient temperature of the laboratory during the experiments (21 °C)	~60 (0.2 SDS)	16.6	1,171	39.9
	~80 (0.05 SDS)	77	1,218	55.8
	~80 (0.2 SDS)	77	1,218	48.2

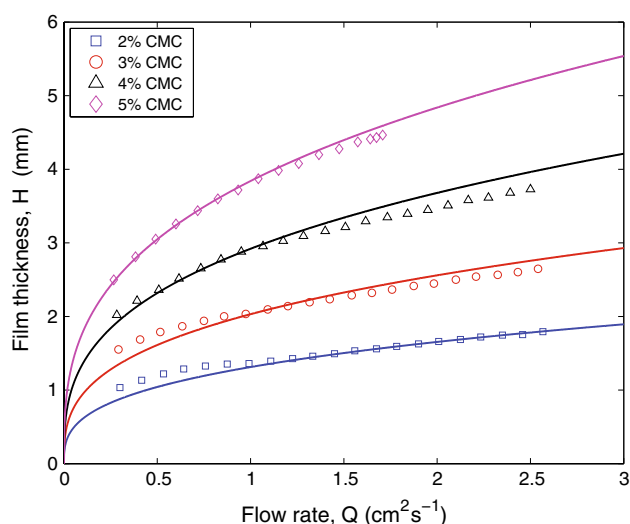


Fig. 6 Film thickness versus flow rate for 2, 3, 4 and 5 % CMC solutions. The data points correspond to experimental measurements, whilst the *solid lines* plot the predicted thickness from Eq. (1). Measurements taken 10 mm downstream of the exit region ($Re = 0.034 - 6.75$)

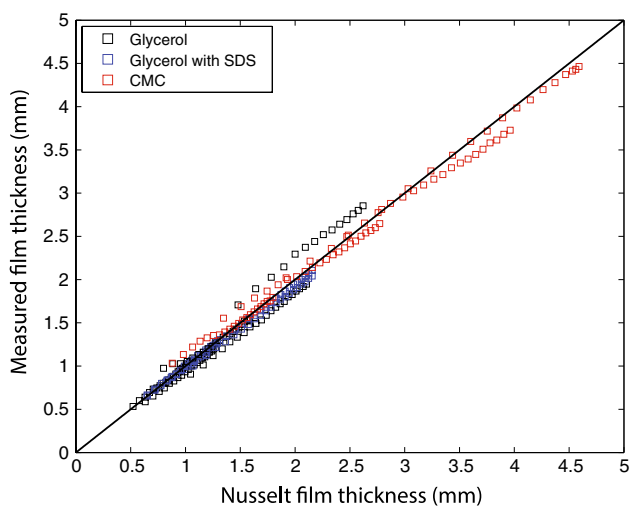


Fig. 7 Comparison of film thickness measurements versus the exact Nusselt solution (Eq. 1). The plot includes all one-layer experiments, a total of 262 measurements with $Re = 0.034 - 34$

solution (Eq. 1) assumes the zero-shear viscosities (i.e. $\mu_0 = 37, 137, 407$ and 926 mPa s) as the constant viscosity, which yields excellent agreement and thus indicates that the shear-thinning characteristics can be neglected in the one-layer flow. Taking, as a first approximation, an average shear rate $\dot{\gamma} \approx U_s/h = O(10 \text{ s}^{-1})$, and using Eq. (3) and values in Table 2, this would lead to a negligible reduction in viscosity for all but the 4 and 5 % CMC solutions at high-flow rates, where we do observe a very slight overestimate of the film thickness.

In general, we found excellent agreement between the one-layer experiments and the Nusselt solution (1), as shown in Fig. 7, where all of the data acquired from the one-layer experiments are plotted in the form of the experimental measurements for the film height versus the Nusselt solution. This comprises a total of 262 experimental conditions (flow rates and viscosities, etc.). It is clear to see that the data collected from the experiments agree excellently with the theory, for all of the solutions used. Noting that these film thicknesses were taken downstream of the exit slot, this is to be expected as the film flow has reached a fully developed steady state.

The same conclusion is reached when considering a two-layer film, where both layers are comprised of the same fluid (so that the only difference between layers is the respective flow rate, i.e. differential motion). The multi-layer approximation by Jiang et al. (2005) given by Eq. (2) essentially predicts that a multi-layer film behaves the same as a one-layer film. For example, this means that a two-layer film with flow rates in the bottom and top layers given by $Q_1 = 1.5 \text{ cm}^2 \text{ s}^{-1}$ and $Q_2 = 0.5 \text{ cm}^2 \text{ s}^{-1}$ theoretically has the same total film thickness and velocity profile as that of a single layer with a flow rate $Q = 2 \text{ cm}^2 \text{ s}^{-1}$, implying that the one-layer approximation given by Eq. (2) should predict the total film thickness for two- and three-layer films exactly. Two such cases depicting this are shown in Fig. 8a, b, showing the total flow rate plotted against total film thickness, where both layers are (a) 70 % glycerol and (b) 4 % CMC. The solid black line shows the simple one-layer approximation from Eq. (2), whilst the data points show a variety of different experimental data—where either the flow rate in the bottom layer was fixed and the flow rate in the top layer was varied or vice versa (see legend for details). In both cases, and for both fluids, it can be seen that the one-layer approximation describes the thickness precisely across the whole range of flow rates.

In Fig. 9, we plot all of the experimental data from two-layer experiments (a total of 833 measurements) to compare against the one-layer approximation, where there is clearly a very good fit between the data and the theory, despite some slight discrepancies for the higher viscosity glycerol solutions with $h > 2$ mm. Thus, for one- and two-layer films of the same liquid, the Nusselt solution (1) and approximation (2), respectively, provide excellent analytical descriptions of the film thickness.

For two-layer films of different fluids, we observe some minor discrepancies with the one-layer film approximation, depending on which fluid is in the bottom layer closest to the wall. This is evident with reference to Fig. 10, where we plot the raw values of film thicknesses for two-layer experiments with 60 and 80 % glycerol versus flow rate. Clearly, there is a larger

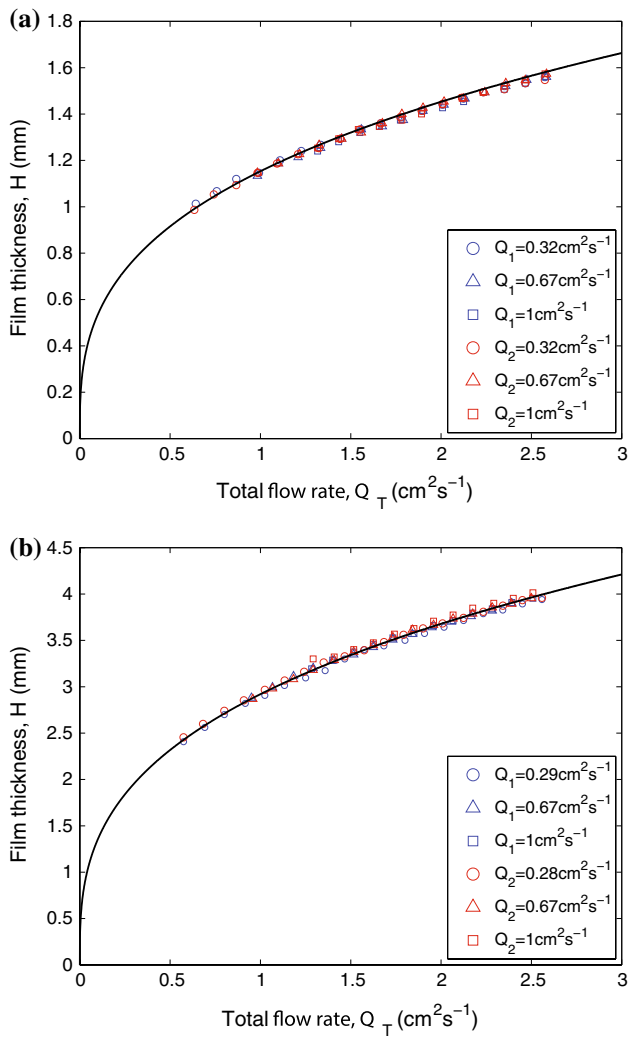


Fig. 8 Total film thickness versus total flow rate for two-layer film flows where both layers are (a) 70 % glycerol and (b) 4 % CMC. The legend indicates which layer had a fixed flow rate, whilst the other layer’s flow rate was varied. The solid black curve shows the one-layer approximation. Reynolds numbers are (a) $Re = 2.4 - 10.4$ and (b) $Re = 0.15 - 0.64$

discrepancy when the more viscous fluid is in the bottom layer (i.e. blue data points) and with a higher flow rate in the top layer, which may be partly due to streamwise developments in the flow for this case (see discussion in Sect. 5 for more details). In spite of this, regardless of which fluid is in the top or bottom layer, the one-layer approximation deviates from the experimental data up to a maximum of 20 % for the highest flow rates, again showing that Eq. (2) provides a reasonable description even for films where the individual layers have different properties. To our knowledge, these data represent the first such verification of the analytical description for multi-layer films.

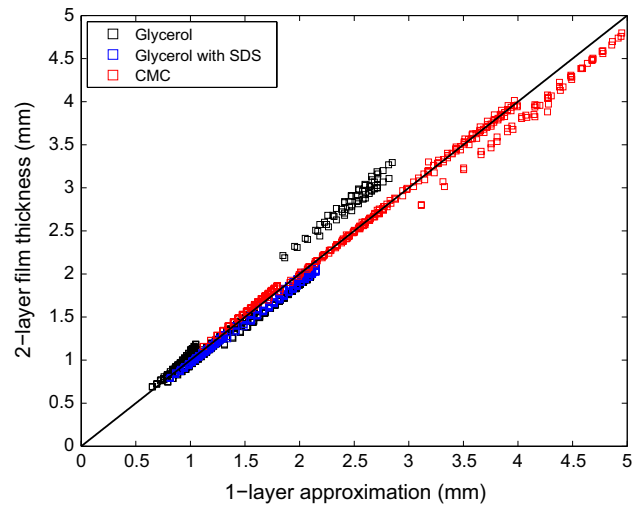


Fig. 9 Comparison of film thickness measurements versus the one-layer approximation (Eq. 2). The plot includes all two-layer experiments, a total of 883 measurements ($Re = 0.065 - 35$)

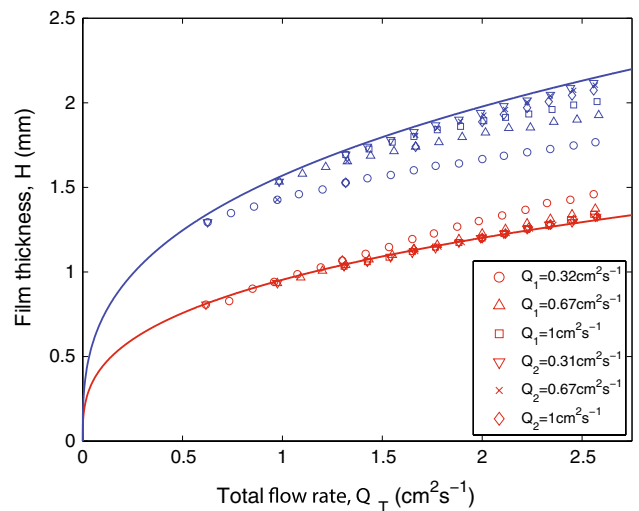


Fig. 10 All of the two-layer experiments plotted where one layer is 60 % glycerol with 0.2 % SDS, and the other is 80 % glycerol with 0.2 % SDS. The red data points indicate when the 60 % solution was the bottom layer; The blue when the 80 % solution was the bottom layer. The layer that had a fixed flow rate is indicated in the legend. The solid lines show the predicted thickness from the one-layer approximation ($Re = 1.0 - 19.9$)

4 Flow velocity measurements

Some example velocity fields, determined as per the method outlined in Sect. 2, are shown in Fig. 11 for a 4 % CMC solution at various flow rates (see caption for details). Note that the velocity scale ($|v| \in (0, 0.08)$ m/s) is the same for all images. In all cases, we observe qualitatively similar features, whereby the flow velocity exhibits a parabolic

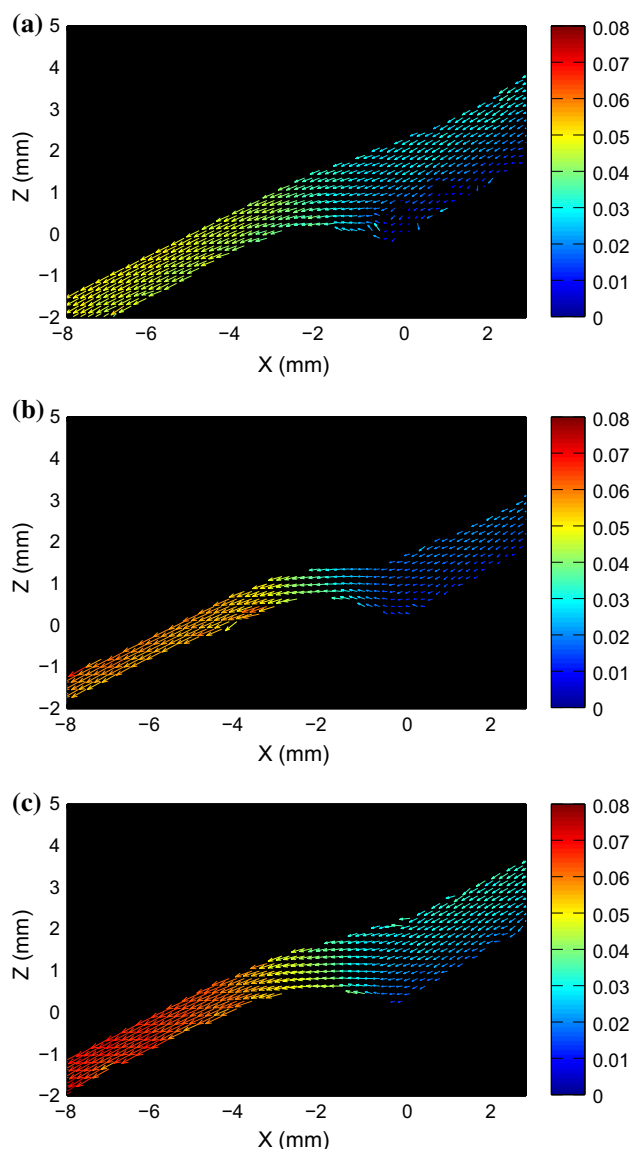


Fig. 11 Velocity fields measured near the exit slot of layer one (location A in Fig. 1). The origin $(x, y) = (0, 0)$ corresponds to the back of the exit slot at the face of the die. The velocity scale is in m/s. Flow rates are (a) $Q_1 = 0.5 \text{ cm}^2 \text{ s}^{-1}$, $Q_2 = 0.5 \text{ cm}^2 \text{ s}^{-1}$, $Re = 0.25$ (b) $Q_1 = 1 \text{ cm}^2 \text{ s}^{-1}$, $Q_2 = 0.3 \text{ cm}^2 \text{ s}^{-1}$, $Re = 0.32$ and (c) $Q_1 = 1 \text{ cm}^2 \text{ s}^{-1}$, $Q_2 = 0.5 \text{ cm}^2 \text{ s}^{-1}$, $Re = 0.37$

distribution normal to the die face before the two layers merge and thereafter, the top layer assumes a more constant velocity. The distance downstream of the exit slot in order for the top layer to reach this constant velocity is approximately 5–7 mm for most cases. In the remainder of this section, we present measurements of the surface velocity *and* velocity as a function of distance perpendicular to the die face.

Firstly, considering two-layer films, Fig. 12 shows two different experimental conditions. In both, the blue vertical dashed lines correspond to the predicted location of the

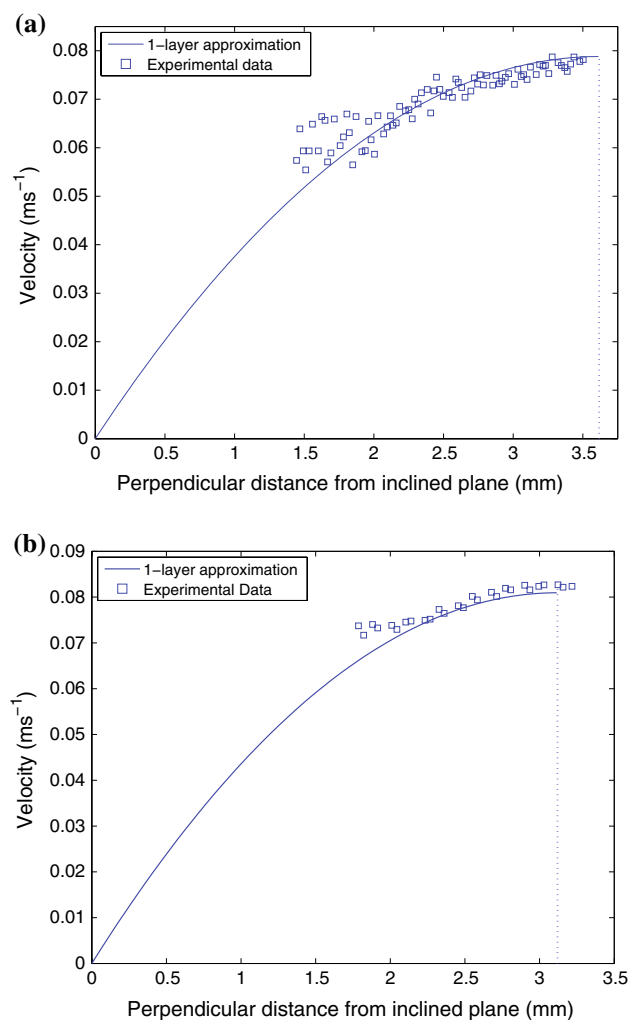


Fig. 12 Plots of the velocity versus perpendicular distance from the die face for two-layer films. In (a), both layers are 4 % CMC with $Q_1 = 0.5 \text{ cm}^2 \text{ s}^{-1}$, $Q_2 = 1.4 \text{ cm}^2 \text{ s}^{-1}$ ($Re = 0.47$); in (b), both layers are 90 % glycerol with $Q_1 = 0.68 \text{ cm}^2 \text{ s}^{-1}$, $Q_2 = 1.01 \text{ cm}^2 \text{ s}^{-1}$ ($Re = 0.96$)

free surface. Since the flow is seeded with hydrogen bubbles only in the top layer and that buoyancy is negligible, we would expect our measurements to coincide with these limits, which is indeed the case. In all cases, we find that despite the relatively small range of velocities, there is a favourable comparison between the velocity distribution in Eq. (1) and experiments.

Furthermore, as well as determining the velocity profile along a line perpendicular to the die face, the free surface velocity can be extracted along the profile of the film that is imaged, i.e. both upstream and downstream of the exit slot. Figure 13 depicts this; upstream of the exit slot ($x > 0$) the film is a single layer, with the theoretical free surface velocity given by the lower dashed horizontal line. Then, the two layers merge to form a two-layer film at $x = 0$,

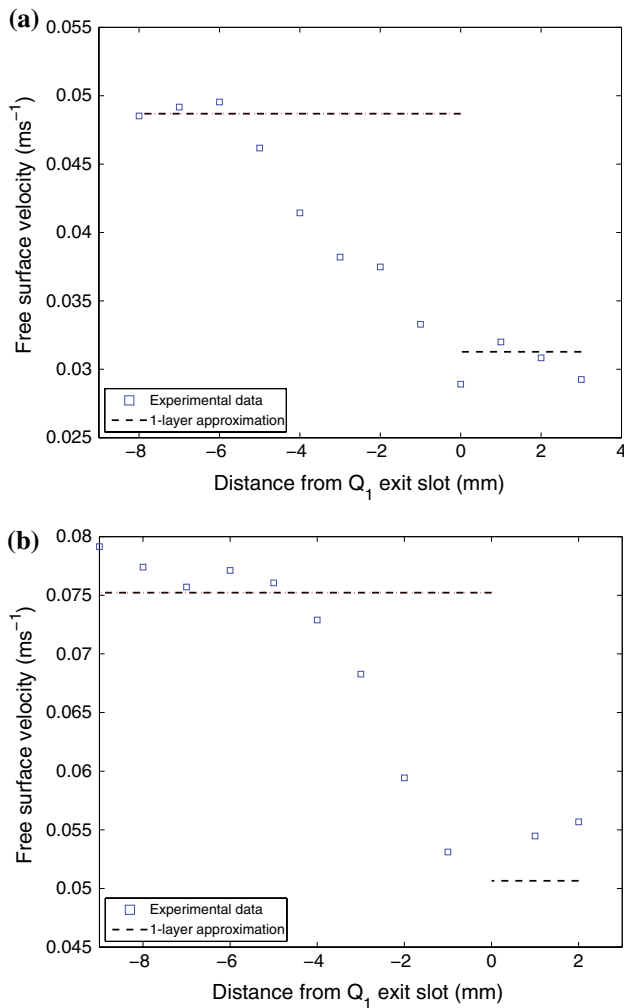


Fig. 13 Plots of the free-surface velocity against streamwise distance from exit slot 1 ($x < 0$ is upstream) for two-layer flows. The *dashed lines* correspond to theoretical predictions, the data points to experiments. In (a), both layers are 5 % CMC with $Q_1 = 0.68 \text{ cm}^2 \text{ s}^{-1}$, $Q_2 = 0.72 \text{ cm}^2 \text{ s}^{-1}$ ($Re = 0.15$); in (b), both layers are 90 % glycerol with $Q_1 = 0.68 \text{ cm}^2 \text{ s}^{-1}$, $Q_2 = 0.83 \text{ cm}^2 \text{ s}^{-1}$ ($Re = 0.86$)

after which we observe an increase in free-surface velocity until approximately 6 mm downstream ($x = -6$) when the free-surface velocity plateaus around 4.7 and 7.5 cm/s in Fig. 13a, b, respectively, which are very close to the theoretical free-surface velocities at this point (shown by the upper dot-dash lines in both plots).

To summarise, Fig. 14 plots all measurements of the free-surface velocity for two-layer experiments, where the measurements upstream (technically for single layer) have also been included. It is clear that Eq. (2) provides a very accurate description across the broad range of parameters ($Re = 0.03 - 1.8$) used herein.

The equivalent analysis for three-layer films is shown in Figs. 15 and 16, respectively. In Fig. 15, we find that Eq. (2) describes the experimental data extremely well in

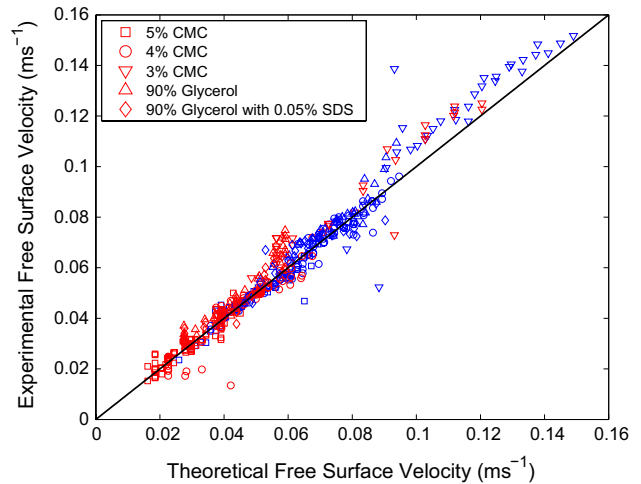


Fig. 14 Theoretical prediction of the free surface velocity plotted against experimental values for all two-layer film flows. Different symbols correspond to the different fluids ($Re = 0.03 - 1.8$)

both (a) and (b), though the theory does show a slight overestimate of the experimental data. These same trends are also displayed in the free-surface velocities, measured as a function of distance upstream/downstream of the exit slot, shown in Fig. 16, where the free-surface velocity downstream is described well by the theory, despite a consistent overestimate of the upstream data, emphasised particularly in (b).

5 Capillary ridge formation

Throughout the course of these experiments, we observed a small ridge/dimple formation on the free surface for the lowest viscosity fluids ($\mu = 8.4$ and 15.3 mPa s). However, as mentioned in Sect. 2, we conclude that these are not waves as the images were taken with a sufficiently long exposure (1 s) so that any waves would appear blurry in the images since $U_s = O(\text{cm/s})$, meaning that the crest of a wave would travel several centimetres during the exposure time. This is clearly not the case, as shown in Fig. 17. This image demonstrates a relatively large capillary ridge just prior to the exit slot region, which is both preceded and followed by a dimple. This free-surface profile formation was observed in numerical studies for a film flow over a “step-in” feature, described in detail by Bontozoglou and Serifi (2008).

Using simple edge-detection routines, free surface profiles such as that shown in Fig. 17 can be easily digitised and are plotted in Fig. 18 for 50 % [(a) and (b)], 60 % [(c) and (d)] and 70 % [(e) and (f)] glycerol ($\mu = 8.4, 15.3$ and 30 mPa s). These plots are all of two-layer films, located at the first layer exit slot, i.e. where the top layer first meets

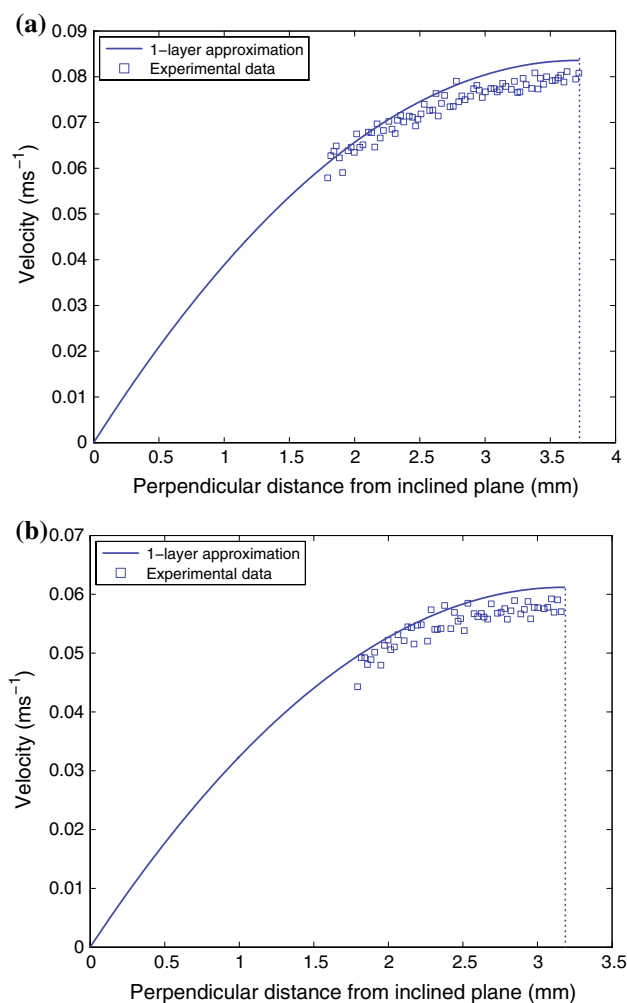


Fig. 15 Plots of the perpendicular distance from the die face against velocity for three-layer films. All layers are 4 % CMC with (a) $Q_1 = 0.67 \text{ cm}^2 \text{ s}^{-1}$, $Q_2 = 0.33 \text{ cm}^2 \text{ s}^{-1}$, $Q_3 = 1.08 \text{ cm}^2 \text{ s}^{-1}$ ($Re = 0.51$); And (b) $Q_1 = 0.5 \text{ cm}^2 \text{ s}^{-1}$, $Q_2 = 0.5 \text{ cm}^2 \text{ s}^{-1}$, $Q_3 = 0.3 \text{ cm}^2 \text{ s}^{-1}$ ($Re = 0.32$). Note again how the three-layer theory matches the one-layer approximation

the bottom layer and the transition from a single-layer film to a two-layer film occurs (location A in Fig. 1). The vertical black lines correspond to the location of the exit slot, with the origin (0 mm from the slot) defined as the point at which the exit slot begins. The film heights were measured as if the inclined plane was 30° for the whole of the die face, without an exit slot region, so the film thickness in between these vertical lines is not a wholly accurate measure of the actual thickness, but plotted for completeness. The particular feature to note, however, is the ridge and/or dimple which occur before the exit slot, i.e. $x < 0$, which is most readily observed in Fig. 18a.

In Fig. 18a, c, e, the bottom layer flow rate, Q_1 , is fixed (at 0.31 or $0.32 \text{ cm}^2 \text{ s}^{-1}$ in each case) and each plot indicates the difference when the top layer, Q_2 , is varied. It can

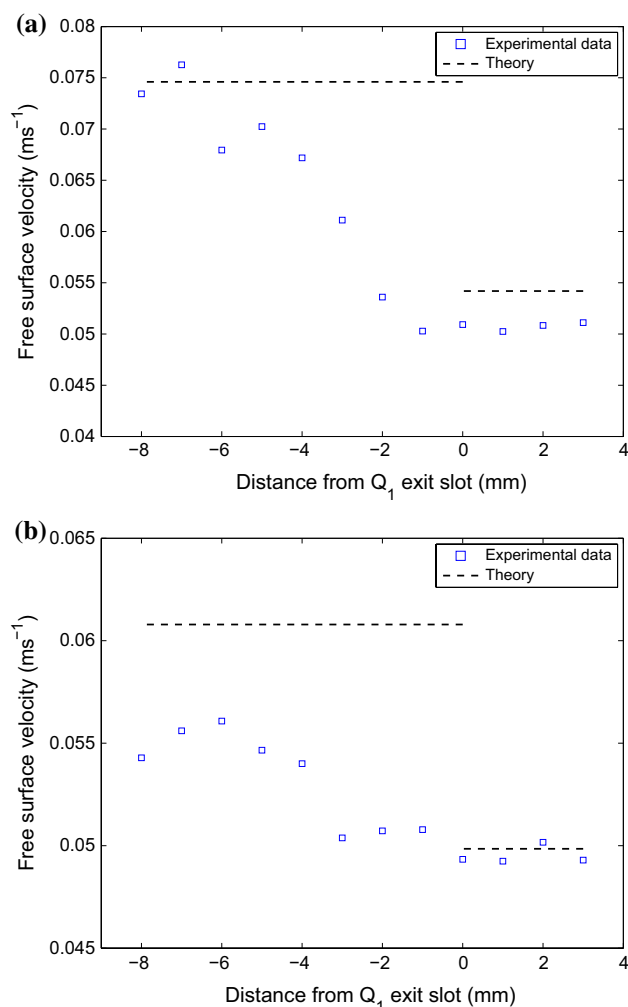


Fig. 16 Plots of the free-surface velocity against streamwise distance from exit slot 1 ($x < 0$ is upstream) for three-layer films. In (a), all layers are 4 % CMC with $Q_1 = 0.67 \text{ cm}^2 \text{ s}^{-1}$, $Q_2 = 0.33 \text{ cm}^2 \text{ s}^{-1}$, $Q_3 = 1.08 \text{ cm}^2 \text{ s}^{-1}$ ($Re = 0.51$); And (b) all layers are 5 % CMC with $Q_1 = 0.5 \text{ cm}^2 \text{ s}^{-1}$, $Q_2 = 0.5 \text{ cm}^2 \text{ s}^{-1}$, $Q_3 = 0.94 \text{ cm}^2 \text{ s}^{-1}$ ($Re = 0.21$)

be seen, in particular for Fig. 18(a), that before reaching the exit slot for layer one, the free surface exhibits a pronounced capillary ridge formation, whereby the free surface goes from being almost uniform 10 mm upstream, to having a wave-like pattern just a few millimetres from the exit slot. This effect is exaggerated when Q_2 is increased, due to an increase in the Reynolds number, as also described in Bontozoglou and Serifi (2008). In accordance with this, as the viscosity is increased, these disturbances are damped out as can be seen in the comparison between Fig. 6a and c or e. After the exit slot region (approximately 5.5 mm downstream), the film is now two layers and returns to a more or less uniform thickness (discussed in more detail later).

In plots (b), (d) and (f), Q_2 is fixed (at either 0.31 or $0.32 \text{ cm}^2 \text{ s}^{-1}$) and Q_1 is varied as indicated in the legends.

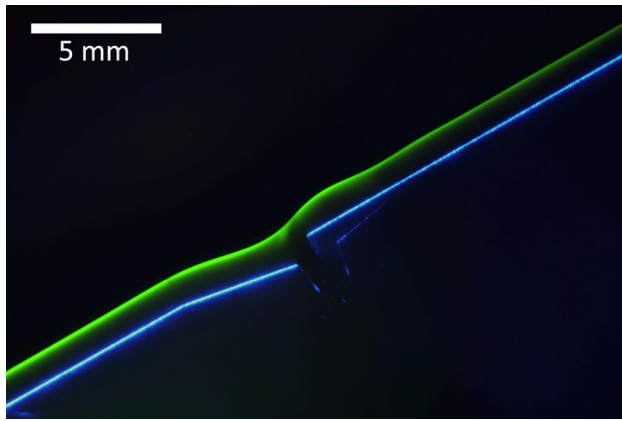


Fig. 17 Raw experimental image showing the free surface of a two-layer flow near the exit slot region of Q_1 . The die face has been superimposed on the image for reference. The flow rates here are $Q_1 = 0.31 \text{ cm}^2\text{s}^{-1}$ and $Q_2 = 2.25 \text{ cm}^2\text{s}^{-1}$. $Re = 35$. Only the free surface is visible here, not the interface between the *top* and *bottom* layers. A capillary ridge is clearly seen before the layers meet

Focusing on Fig. 18b, however, despite all profiles having the same uniform thickness upstream ($x \approx -10 \text{ mm}$), a dimple formation appears at $x \approx -4 \text{ mm}$ for the highest flow rates ($Q_1 = 1.81$ or $2.26 \text{ cm}^2\text{s}^{-1}$) before rising rapidly to meet the flow coming from the exit slot. Notice that the location of the dimple occurs progressively closer to the exit slot as flow rate decreases and, in particular, there is a transition from dimple to ridge as $Q_1 = 0.31 \text{ cm}^2\text{s}^{-1}$ followed by a dimple occurring *inside* the exit slot region. Again, the magnitude of this effect is damped out as the viscosity increases. Our observations of ridges are summarised in Fig. 19, where we plot the normalised ridge height versus Reynolds number. Interestingly, we observe the data for both 50 and 60 % glycerol solutions collapses and that there is a local maximum occurring at $Re \approx 25$, which

In our experiments, due to the geometry of the exit slot, we have an extension of the “step-in” capillary ridge formation for low flow rates in Q_1 , described by Bontozoglou and Serifi (2008). For our geometry, when there is a low flow rate in Q_1 , the flow from Q_2 essentially sinks down into the exit slot region, inducing a component of velocity normal to the free surface, which results in a small reduction in the streamwise velocity and thus a local high-pressure region, which would result in a pressure gradient back towards the direction of the incoming flow from Q_2 . As such, one would expect a small thickening of the film just prior to the exit region, which is precisely what we observe.

In contrast, for high-flow rates in Q_1 we essentially have an extension of the “step-out”, where the opposite would be true, inducing a dimple in the top layer before the two layers merge, which is again precisely what we observe in the experimental profiles shown in 18.

In the work by Bontozoglou and Serifi, the film flow over step-in or step-out features was vertical. They showed that the size of the capillary ridges initially grows with Reynolds number, but then diminishes. Two limits were identified as follows: a low Reynolds number limit, whereby the streamwise deformations are expected to follow the simple scaling law $l = L/H = Ca^{-1/3}$, where L is the streamwise scale of the deformation, H is the undisturbed film thickness and $Ca = \rho g H^2 / \sigma$ is the Capillary number. In the high- Re limit, where inertia dominates, the deformations are expected to follow the scaling $l = We^{-1/2} = (\rho H U^2 / \sigma)^{-1/2}$. A quick inspection of Fig. 18a for example shows that the streamwise lengthscale is of the order of 2 mm immediately prior to the step-in. The streamwise lengthscale being the total length of the ridge which resides above the upstream uniform thickness. In this high- Re case ($Re = 30.7$), the predicted lengthscale is $L = H(\rho H U^2 / \sigma)^{-1/2} = 3.5 \text{ mm}$, showing a relatively large quantitative discrepancy; however, the orientation of the flow is different and, for our experiments, flow emanates from the exit slot, which was not the case in the study by Bontozoglou and Serifi. A full analysis of the ridge and dimple formation in two-layer film flows is the subject of ongoing work.

Furthermore, the predictions from the numerical study for step-ins showed that as Re increases, the ridge is transformed into a series of damped stationary capillary waves. This certainly appears in the experiments; for example in Fig. 18a, as the flow rate is increased, we observe a progression from a single ridge ($Q = 0.31 \text{ cm}^2\text{s}^{-1}$) to a series of stationary waves reaching farther upstream ($Q = 1.8$ and $2.25 \text{ cm}^2\text{s}^{-1}$). In contrast to the situation where the flow is fully developed and steady state, for this particular feature, surface tension thus becomes important and a higher surface tension would act to increase the size of the capillary ridges or dimples.

Figure 19 plots the normalised ridge height, $h_{\text{ridge}} - H/H$, versus Reynolds number in the top layer (i.e. $Re = \rho Q_2 / \mu_2$). Both fluids (50 and 60 % glycerol mixtures) exhibit an initial increase in ridge height as Re increases, but a definitive local maxima occurs at $Re \approx 25$. This non-monotonic dependence was reported by Bontozoglou and Serifi as being due to the distinction between regimes where viscosity dominates (low Re) and where inertia dominates (high Re), whereby the intermediate regime is where capillary forces dominate and result in a pronounced ridge.

As seen, the profiles tend to a uniform thickness after the two layers merge. However, this does not occur until sufficiently far downstream ($>10 \text{ mm}$ in some cases). As such, in Fig. 20 we compare the film thickness measured in this location to those measured just before the curvature of the die (location B in Fig. 1). Figure 20 does this for the cases

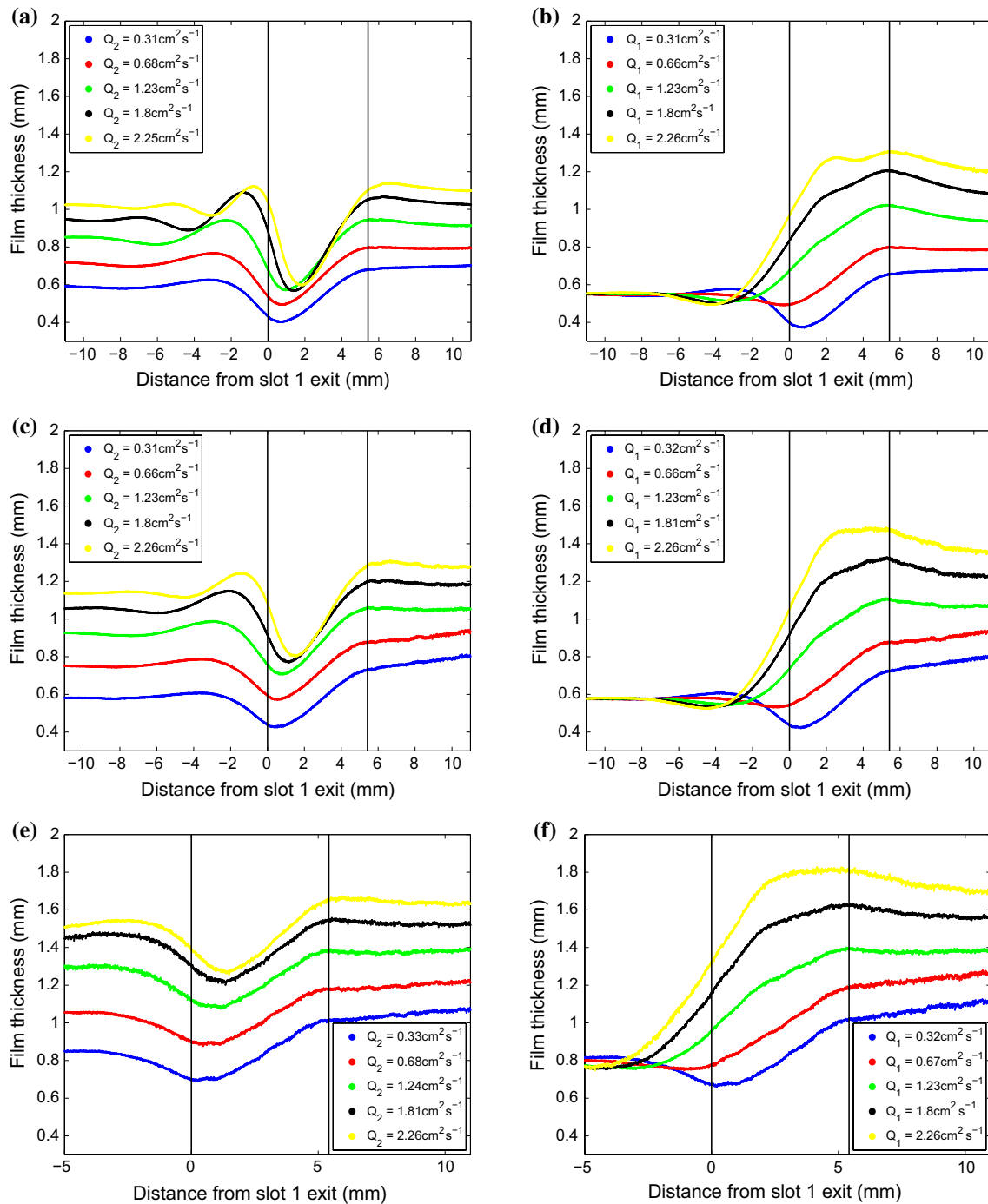


Fig. 18 Free-surface profiles shown as total film height against distance from the exit slot of the first layer (all films comprised of two layers), i.e. the free surface. **a** 50 % glycerol with $Q_1 = 0.31 \text{ cm}^2 \text{ s}^{-1}$ fixed, **b** $Q_2 = 0.31 \text{ cm}^2 \text{ s}^{-1}$ fixed; **c** 60 % glycerol with $Q_1 = 0.32 \text{ cm}^2 \text{ s}^{-1}$ fixed, **d** $Q_2 = 0.31 \text{ cm}^2 \text{ s}^{-1}$ fixed; **e** 70 % glycerol

with $Q_1 = 0.32 \text{ cm}^2 \text{ s}^{-1}$ fixed, **f** $Q_2 = 0.32 \text{ cm}^2 \text{ s}^{-1}$ fixed; In all cases, the converse layer’s flow rate is provided by the legend. For **(a)** and **(b)**, $Re = 8.1 - 34$; for **(c)** and **(d)**, $Re = 4.6 - 19.1$; for **(e)** and **(f)**, $Re = 2.4 - 9.9$

of **(c)** and **(d)** in Fig. 18, considered to be the “least uniform” after the exit slot region. We see in these cases that the measurement of the film thickness just after the exit slot (location A) is consistently lower than the measurement

taken just before the curvature (location B). However, the maximum difference, even for this low-viscosity fluid ($\mu = 15.3 \text{ mPa s}$) is always less than 0.08 mm (<11 % of the film thickness). This consistent thickening of the layer

may be due in part to a streamwise development of the film flow after the layers merge at the exit slot of the bottom layer, imposing a Poiseuille-type velocity profile, which would interact with the upstream film. This appears to be supported by the free-surface profiles, in particular, those shown in Fig. 18(c). Noting that the error in the experimental measurements is small ($\approx O(10) \mu\text{m}$) compared to the film thickness ($\approx O(100) \mu\text{m}$), we thus conclude that this discrepancy is indeed due to a streamwise development of the flow.

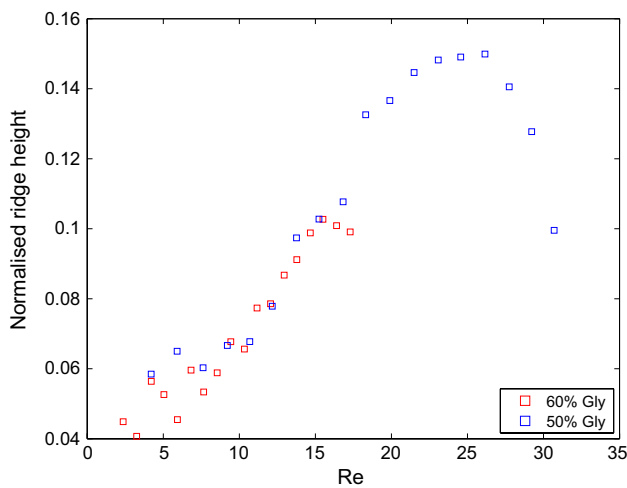


Fig. 19 Normalised ridge height versus Reynolds number

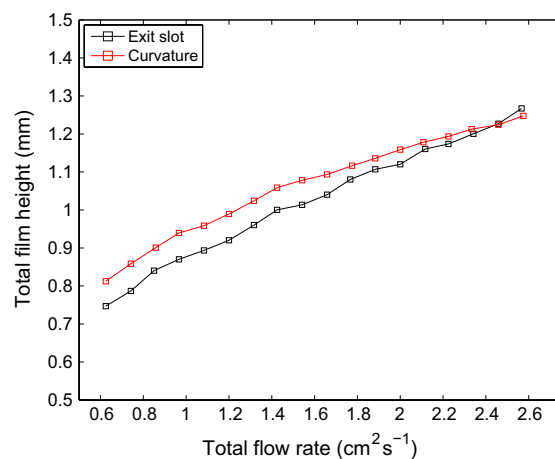
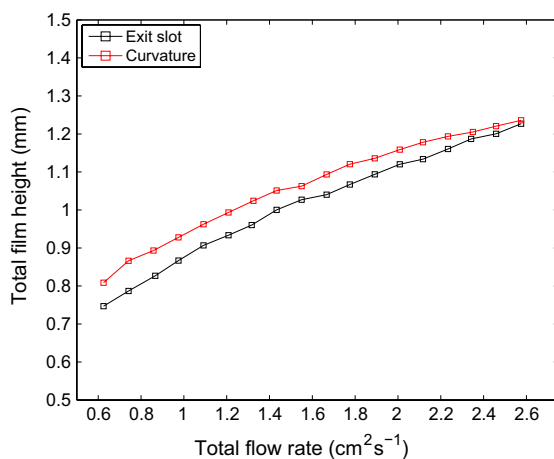


Fig. 20 A comparison of measuring the film heights at different positions along the die. Both plots show the total film height against total flow rate for a two-layer film where both layers are 60 % glycerol, with $Q_1 = 0.32 \text{ cm}^2 \text{ s}^{-1}$ fixed (top), and $Q_2 = 0.31 \text{ cm}^2 \text{ s}^{-1}$ fixed

(bottom). The film thickness was measured in two locations; just after the slot 1 exit (black; at location A in Fig. 1) and further along the die face, just before the change from an inclined plane to a curved surface (red; at B in Fig. 1). $Re = 6.8 - 22.2$

6 Conclusions

In summary, we have completed a thorough experimental study of both single- and multi-layer film flows down an incline plane in order to test the applicability of the one-layer approximation for both film thicknesses and velocity profiles over a range of physical properties and parameters, with $Re \approx 0.03 - 60$. To our knowledge, this is the first such systematic study of multi-layer film flows.

The film thicknesses measured for both single-layer films and two-layer films of the same fluid were described very accurately by the well-established one-layer approximation, whilst a mild discrepancy was noted for two-layer films of different fluids, in particular when the bottom layer was more viscous than the top layer.

Using high-speed imaging, we extracted velocity profiles for both two- and three-layer films, measuring both the velocity as a function of distance from the wall and the free-surface velocity. In the two-layer case, there is again excellent agreement between theory and experiment, whilst for three-layer films, there is good agreement despite a slight overestimate by the theory.

For two-layer films of low-viscosity fluids, we observed the formation of stationary capillary ridges and dimples along the free surface, just prior to the exit slot region where the two layers merge. These formations were described with reference to the work of Bontozoglou and Serifi (2008) for film flows over step-ins and step-outs, whereby the qualitative observations from the present experiments matched accurately with their numerical study. The ridges were found to be most pronounced for low viscosity, high-flow rates (i.e. higher Reynolds numbers),

where the peak ridge is preceded by a series of dimples and ridges of diminishing amplitude. Coupling the size of the ridges with the presence of flow emanating from the exit slot is the subject of ongoing work.

By inspection of the film thickness profiles around the exit slot, we found that the two-layer films generally reach their equilibrium values approximately 11 mm downstream of the exit slot and comparison with the film thicknesses measured a further 40 mm downstream showed a maximum difference of 10 %. This was attributed to a stream-wise development in the flow.

To conclude, we have provided a thorough validation of the one-layer approximation for a range of physical properties and parameters in a true multi-layer film flow. Understanding the flow in the region where layers merge, whereby a liquid–liquid interface is formed, is crucial for the design of components in many coating processes and the data gained from these, and similar, experiments provide the motivation for future work in this area. In particular, future work will focus on both experimental measurements and modelling of the change in heights of the individual layers for multi-layer films, coupled with velocity fields in order to better characterise the ridge and dimple formations.

References

- Adomeit P, Renz U (2000) Hydrodynamics of three-dimensional waves in laminar falling films. *Int J Multiph Flow* 26:1183–1208
- Akhtaruzzaman AFM, Wang CK, Lin SP (1978) Wave motion in multilayered liquid films. *J Appl Mech* 45(1):25–31
- Alekseenko SV, Antipin VA, Bobylev AV, Markovich DM (2007) Application of PIV to velocity measurements in a liquid film flowing down an inclined cylinder. *Exp Fluids* 43:197–207
- Benchabane A, Bekkour K (2008) Rheological properties of carboxymethyl cellulose (CMC) solutions. *Colloid Polym Sci* 286:1173–1180
- Benjamin TB (1957) Wave formation in laminar flow down an inclined plane. *J Fluid Mech* 2:554–574
- Binnie AM (1957) Experiments on the onset of wave formation on a film of water flowing down a vertical plane. *J Fluid Mech* 2:551–553
- Bontozoglou V, Serifi K (2008) Falling film flow along steep two-dimensional topography: the effect of inertia. *Int J Multiphase Flow* 34:737–747
- Chhabra RP, Richardson JF (2008) *Non-newtonian flow and applied rheology*, 2nd edn. Butterworth-Heinemann, Oxford
- Christodoulou KN, Scriven LE (1984) AICHE Annual Meeting, San Francisco, CA, Paper 1423
- Clarke A (1995) Application of particle tracking velocimetry and flow visualisation to curtain coating. *Chem Eng Sci* 50:2397–2407
- Dietze GF, Al-Sibai F, Kneer R (2009) Experimental study of flow separation in laminar falling liquid films. *J Fluid Mech* 637:73–104
- Drosos EIP, Paras SV, Karabelas AJ (2004) Characteristics of developing free falling films at intermediate Reynolds and high Kapitza numbers. *Int J Multiph Flow* 30:853–876
- Jiang WY, Helenbrook BT, Lin SP, Weinstein SJ (2005) Low-Reynolds-number instabilities in three-layer flow down an inclined wall. *J Fluid Mech* 539:387–416
- Kalliadasis S, Bielarz C, Homsy GM (2000) Steady free-surface thin film flow over two-dimensional topography. *Phys Fluids* 12:1889–1898
- Kao TW (1965a) Stability of two-layer viscous stratified flow down an inclined plane. *Phys Fluids* 8(5):812–820
- Kao TW (1965b) Role of the interface in the stability of stratified flow down an inclined plane. *Phys Fluids* 8(12):2190–2194
- Kao TW (1968) Role of viscosity stratification in the stability of two-layer flow down an incline. *J Fluid Mech* 33:561–572
- Kapitza PL (1948) Wave flow of thin viscous fluid layers. *Zh Eksp Theor Fiz* 18:3–28 (in Russian)
- Kistler SF, Schweizer PM (eds) (1997) *Liquid film coating*. Chapman & Hall, London
- LaPorte RJ (1997) *Hydrophilic polymer coatings for medical devices: structure/properties, development, manufacture and applications*. CRC Press, Boca Raton, FL
- Marston JO, Simmons MJH, Decent SP (2007) Influence of viscosity and impingement speed on intense hydrodynamic assist in curtain coating. *Exp Fluids* 42:483–488
- Marston JO, Thoroddsen ST, Thompson J, Blyth MG, Henry D, Uddin J (2014) Experimental investigation of hysteresis in the break-up of liquid curtains. *Chem Eng Sci* 117:248–263
- Miyamoto K, Katagiri Y (1997) Curtain coating. In: Kistler SF, Schweizer PM (eds) *Liquid film coating Ch 11c*. Chapman & Hall, London
- Njifenju AK, Bico J, Andres E, Jenffer P, Fermigier M (2013) Experimental investigation of liquid films in gravity-driven flows with a simple visualization technique. *Exp Fluids* 54:1506
- Noakes CJ, Gaskell PH, Thompson HM, Ikin JB (2002) Streak-line defect minimization in multi-layer slide coating systems. *Chem Eng Res Des* 80(5):449–463
- Nusselt W (1916) Die oberflächenkondensation des wasserdampfes (in German) *Z Ver Dt Ing* 60:541–552 (English translation by D. Fullarton, *Chem. Eng. Fund.* 1, 6–19 (1982))
- Portalski S (1963) Studies of falling liquid film flow. *Chem Eng Sci* 18:787–804
- Salazar RP, Marschall E (1978) Time-average local thickness measurement in falling liquid film flow. *Int J Multiph Flow* 4:405–421
- Schweizer PM (1988) Visualization of coating flows. *J Fluid Mech* 193:285–302
- Wang CK, Seaborg JJ, Lin SP (1978) Instability of multilayered liquid films. *Phys Fluids* 21(10):1669–1673
- Weinstein SJ (1990) Wave propagation in the flow of shear-thinning fluids down an incline. *AIChE J* 36:1873–1889
- Weinstein SJ, Ruschak KJ (2004) Coating flows. *Annu Rev Fluid Mech* 36:29–53
- Wierschem A, Scholle M, Aksel N (2002) Comparison of different theoretical approaches to experiments on film flow down an inclined wavy channel. *Exp Fluids* 33:429–442
- Yih C-S (1955) In: *Proceedings 2nd U.S. National Congress Applied Mechanics*, p 623. American Society of Mechanical Engineers, New York
- Yih C-S (1963) Stability of liquid flow down an inclined plane. *Phys Fluids* 6(3):321–334